Chemical Engineering Journal 161 (2010) 223–233

Contents lists available at ScienceDirect

Chemical Engineering Journal

journal homepage: www.elsevier.com/locate/cej

Iterative learning parameter estimation and design of SMB processes

Junghui Chen*, Minghui Chen, Lester Lik Teck Chan

R&D Center for Membrane Technology and Department of Chemical Engineering, Chung-Yuan Christian University, Chung-Li 320, Taiwan, ROC

ARTICLE INFO

Article history:
Received 25 September 2009
Received in revised form 11 April 2010
Accepted 15 April 2010

Keywords:
Iterative learning design
On-line parameter estimation
Physical/empirical based design
Simulated moving bed

ABSTRACT

The simulated moving bed (SMB) is a continuous separation chromatography process. The design of the SMB operation condition is crucially important as it affects the purity of the products. For the physical model based design, the parameters of the system are a pre-requisite and are determined in an offline experiment. More often than not, changes in the operation of the process mean the offline determined parameters may no longer be a true reflection of the process and need to be re-determined. In this work, a novel design strategy which combines the physical-based and the empirical based design in an iterative learning scheme is proposed. In the physical based design, the parameters of the physical model are recalculated through an on-line scheme which makes use of the current on-line measured data from the UV signals obtained in the real process. Using the standing wave equations, the obtained parameters are then used to design the operation condition. With new sets of measurements, the model parameters are refined and the operation condition is also updated until the parameters converge. To overcome the model structure mismatch, the empirical based design is employed for fine improvement. The differences between the desired output and the actual output are used to modify the flow rates until the goal is attained. By a sequence of the two-phase design, the desired quality can be attained systematically. The proposed method is applied to a virtual eight-column SMB process to verify the effectiveness of the proposed method.

1. Introduction

The simulated moving bed (SMB) is a continuous separation chromatography process. The underlying principle of chromatography is different relative adsorption affinities of different components in the solvent, resulting in different migration rates and separation. A conventional SMB consists of four or more columns connected together with two inlets and two outlets. The mixture to be separated enters at the feed port and the separated products are collected at the extract port and raffinate port respectively. The four ports are switched periodically in the direction of the flow which simulates a counter-current movement. It has since attracted interest in the purification of biochemical and pharmaceutical products. Compared to the conventional batch chromatography, SMB offers the advantage of high throughput per bed volume, low solvent consumption, high purity and high yield [1].

One of the key areas in the design of SMB is the determination of zone flow rates and the switch time of the SMB process. In the design of SMB, Storti et al. [2] has proposed a shortcut design tool called the triangle theory. Their key operating parameters were defined as the ratio of the net fluid to solid phase flow rates in each section of the SMB unit. Nevertheless, to reach a specific required purity, trial and error was needed. This method did not relate the purity explicitly to the design criteria, such as the zone flow rates, and solid phase speed. Ma and Wang [3] have proposed the standing wave design for SMB processes. The standing wave design made use of the idea that separation could be achieved if the key concentration wave in each zone migrated at the same speed as the periodic port movement. The product purities are thus link to the flow rates of each zone and the equivalent moving bed velocities.

Optimization of SMB processes was a challenging task, particularly when a rigorous first-principle process model was used [4]. SMB processes exhibit strong non-linear behaviors and they are of periodic nature. Model based optimization strategies are, therefore, of great importance to researchers and practitioners. Kawajiri and Biegler [5] applied nonlinear programming (NLP) to optimization of the SMB process. The partial differential algebraic equations describing the system were fully discretized in both temporal and spatial domains and the optimization was done through an NLP solver. Zhang et al. [6] solved the multi-objective optimization of the simulated moving bed using a genetic algorithm. In their work, the role of various parameters on the performances of a simulated moving bed was investigated using an equilibrium stage model and the purity of the extract and productivity of the unit were simultaneously maximized.

* Corresponding author. Tel.: +886 3 2654107; fax: +886 3 2654199.
E-mail address: jason@wavenet.cycu.edu.tw (J. Chen).

1385-8947/$ – see front matter © 2010 Elsevier B.V. All rights reserved.
doi:10.1016/j.cej.2010.04.027

Nomenclature

C_i^j	concentration in the mobile phase (mg l^{-1})
C_i^{*j}	equilibrium concentration (mg l^{-1})
$\bar{C}$	averaged concentration (mg l^{-1})
D_i	apparent axial dispersion coefficient (cm^2 min^{-1})
D_p	pore diffusion coefficient (cm^2 min^{-1})
e	error between measurement and desired purity
F_c	feed component ratio
H_i	Henry constant
k	number of switch
K	correcting factor
k_{fi}	lumped mass transfer coefficient of component i (min^{-1})
k_i	film mass transfer coefficient (cm min^{-1})
L	column length (cm)
N	number of sampling time
NLP	nonlinear programming
P	bed phase ratio
P^{Ext}	extract purity
P^{Raf}	raffinate purity
$\mathbf{P}^{\mathrm{set}}$	desired purity vector
q_i^j	concentration in the solid phase (mg l^{-1})
RGA	relative gain array
S	surface area (cm^2)
SMB	simulated moving bed
SVD	singular value decomposition
TMB	true moving bed
T_s	switching period (min)
τ	time point within a single switch (ml min^{-1})
t_s	Sampling interval (min)
u^j	zone flow rate (ml min^{-1})
v	solid flow rate in TMB (ml min^{-1})
V	characteristic matrices determined variables
x	axial length (cm)

Greek letters

β	index of product purity
ε	voidage

Superscripts and subscripts

Ext	extract
Raf	raffinate
b	bed
i	index of components, A and B
j	zone number
p	particle
z	index for extract and raffinate

Regardless of the design paradigms, the design methods count on the actual parameters. Parameter estimation for adsorption isotherms, mass transfer coefficients, etc. has been carried out using an offline experimental method. Often, in the operation of the process, the process decay, or inaccurate description of process characteristics means the offline determined parameters may no longer be a true reflection of the process and they need to be re-determined. From a practical point of view, the most effective way is to do parameter estimation and design simultaneously; i.e., the design should be carried out on-line to ensure the designated purity. For on-line design, an intuitive method is used to carry out iterative learning. Information from the previous operation can be used in order to improve the performance via trial to trial in the sense that errors are sequentially reduced. According to Lima and Saraiva [7], by looking at the past records and sets of examples, it is possible to extract and generate important new knowledge. Such an idea has been used widely in control of the process. For example, Heertjes and Tso [8] proposed the use in the lithographic process, and Chen et al. [9], in the pervapration process. For better performance, the physical model used can be augmented with the empirical model.

In SMB design, the knowledge of the position and propagation of wave profiles and the physical parameters is necessary because the position of wave profiles with respect to the position of the inlet and outlet ports determines the quality of the mixture separation. This aim is achieved by the proper choice of the internal flow rates of SMB processes with respect to the switching of the inlet and outlet ports. As physical parameters can be acquired from the previous knowledge, they may not be accurate enough to reflect the current process. In this work, a method is proposed to carry out the parameter estimation and design of the flow rate at the same time. Because the SMB process simulates the counter-flow between the adsorbent and the solvent in a true moving bed (TMB), an analytical solution to the steady state equation for TMB can be used to introduce an approximation of the SMB model solution. With the prior knowledge of the parameters, a set of design conditions is first calculated based on the first-principle model. However, the parameters may not be reflective of the process and with each new set of data, the parameters is recursively updated. These newly obtained parameters reflect the changes of the real environment, equipment or other environmental conditions; thus the error due to parameters inaccuracy is eliminated. Even if the environment does not change, another fact of life is the issue of modeling errors. This is caused by the mathematical representation of SMB involving simplifying assumptions as well as at the measurement position at the moment of the port switching. Because of the model uncertainty in SMB, the design condition should be adjusted to overcome these offsets. To work on the real SMB in real environments, the proposed strategy also incorporates the iterative learning design scheme. The aim is to improve the process from available new data of the process which is the on-line measured data. Although the operation condition can be calculated from the physical model, simplification has been made in the solution and this may affect the actual outcome. To this end, the error is corrected by way of the feedback scheme of the output information.

The remainder of this paper is organized as follows. Section 2 describes SMB operation objectives and lays out the overall design structure. The design procedure is detailed in Section 3. In Section 4, the results from the simulation set-up of the proposed method are presented and discussed. Finally, concluding remarks are made in Section 5.

2. Design objective and structure

The SMB unit under consideration is a standard SMB unit consisting of four sections as shown in Fig. 1. It consists of eight columns arranged in a 2-2-2-2 configuration. The figure shows the first instance when the solvent enters between column 1 and 8, and the feed, between columns 4 and 5. The directions of the successive switches are the same and after 8 switches, i.e. a completion of a cycle, the nodes will return to the same position as the first instance. The SMB unit can be divided into 4 zones. Each zone is constituted of two same volume chromatographic columns. A binary mixture is separated. The more adsorbable component, A, is collected in the extract stream while the less adsorbable one, B, is collected in the raffinate stream. The feed stream is introduced between zones II and III. The desorbent is used to desorb component A from zone I so as to regenerate the adsorbent. Component *B* is adsorbed in zone IV to regenerate the desorbent itself before recycling to zone I.

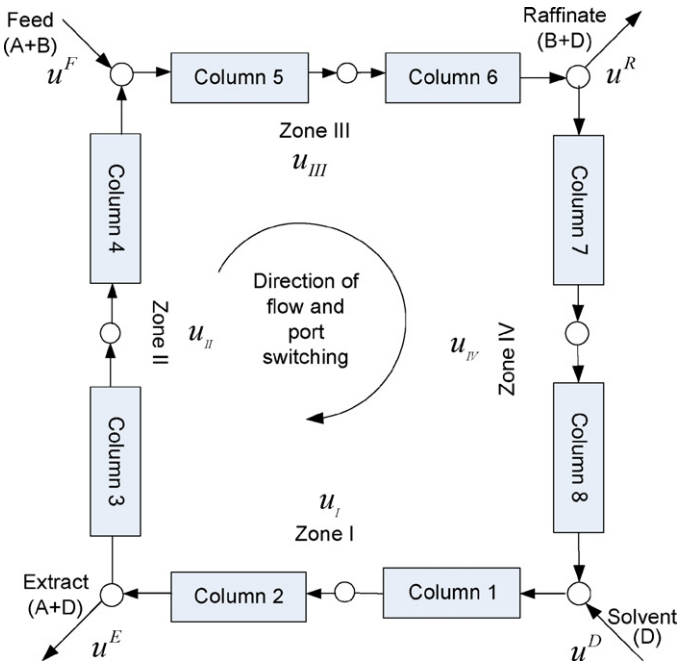

Fig. 1. SMB unit.

The operation of the SMB process aims to separate the mixture into high products purities. The main objectives are the extract purities, P^{Ext} and raffinate purities, P^{Raf}, averaged over one switching period of length T_s. They are defined as

$$
\begin{aligned}
P^{\text{Ext}} &= \frac{\bar{c}_A^{\text{Ext}}}{\bar{c}_A^{\text{Ext}} + \bar{c}_B^{\text{Ext}}} \\
P^{\text{Raf}} &= \frac{\bar{c}_B^{\text{Raf}}}{\bar{c}_A^{\text{Raf}} + \bar{c}_B^{\text{Raf}}} \\
\bar{C}_i^{\text{Ext}} &= \frac{\int_{(k-1)T_s}^{kT_s} C_i^{\text{Ext}}(t)dt}{T_s} \\
\bar{C}_i^{\text{Raf}} &= \frac{\int_{(k-1)T_s}^{kT_s} C_i^{\text{Raf}}(t)dt}{T_s}, \quad i = A, B
\end{aligned}
\tag{1}
$$

The subscript i denotes the components A and B. $C_A^{\text{Ext}}(t)$ and $C_B^{\text{Raf}}(t)$, denote the instantaneous concentration of Component A (more adsorbable) in extract and instantaneous concentration of Component B (less absorbable) in raffinate respectively with $\bar{C}_A^{\text{Ext}}$ and $\bar{C}_B^{\text{Raf}}$ being the average concentration and k is the number of switch.

In order to achieve the defined objective of purities for extract and raffinate, the design scheme proposed is as illustrated in Fig. 2. The scheme is based on iterative learning procedure of the physical model, followed by that of the empirical model. In the physical based design, the solver determines the initial operation based on the prior knowledge of physical models with regard to the desired purity specification, $\mathbf{P}^{\text{set}}=[P^{\text{Ext}}\ P^{\text{Raf}}]^T$ (Fig. 2a). u^j (ml min^{-1}) is the calculated zonal velocities. However, the parameters may not be reflective of the current process. With each new set of data, the parameters are recursively updated and the new operation condition is recalculated based on each newly obtained set of parameters (Fig. 2b). The recursive step is carried out until the parameters converge, indicating that the converged parameters fit the current model structure. However, the design condition will not be accurate when the physical model method is applied and the discrepancy from the target is a result of the process and model mismatch. As a result of the assumptions made in the derivation of the SMB model, any correction that can be made should take the error into account in this mismatch. When the parameters converge, the empirical based design is then applied (Fig. 2c). The errors from the desired and the actual measured outputs of the empirical model are used to correct the current design condition. The corrective variables (zonal velocities) are estimated based on the error ($\mathbf{e}$) of the actual measurement and the desired purity specification, where $\mathbf{K}$ is a correcting weight for the error. This empirical based design can drive the process to the required design specifications.

3. Physical based design

In the physical model based design, the TMB model is used to approximate the SMB process at the cyclic steady state. By reconstructing the wave profile, a regression equation can be derived to update the physical parameters recursively which are then used to calculate the operation condition.

3.1. TMB approximates the SMB profile

The SMB profile can be approximated by the TMB profile when the cyclic steady is attained. Fig. 3 shows TMB and SMB profiles of the four zones under the same condition with the bold lines representing TMB and the thin line representing SMB. The dot dashed line (.-) and the dotted line (..) line represent more absorbable and less absorbable components for the TMB system respectively while those for the SMB system is represented by the solid line and the dashed line (–) respectively. From the figure, it can be observed that the profiles of SMB and TMB in zone I and zone IV can be approximated better than those in zone II and zone III. The TMB profile is a straight line by physical restriction because the TMB concentration reaches a steady state. Thus, the lines in zones II and III do not reflect the concave nature of the profile of SMB in these zones. Therefore, more precise approximation of zone I and zone IV is chosen to construct our wave models.

3.2. Wave reconstruction

To get the output quality of the SMB system, the UV signal is used here. In the past, Ma and Wang [3] employed 8 UV detectors to obtain a complete profile of the SMB unit with 8 nodes. In view of the requirement of the proposed method, 5 UV units will be sufficient for the purpose of parameter estimation. The placement of the UV detectors is shown in the schematic diagram. The extract and raffinate node each has one UV detector for monitoring the purities. The remaining are strategically placed to obtain the boundary concentration for zone I and zone IV as shown in Fig. 4 for a particular instance.

Using ideas of wave front construction presented by Kleinert and Lunze [10], the SMB profile is to be related to the UV measurements. The concentration waves within SMB move at a constant rate within each switch. Using this fact, the moving wave profile of SMB in the time domain is, therefore, related to the static wave profile of TMB in the spatial domain by

$$
C_i^{\text{SMB}}(\tau = nt_s) = C_i^{\text{TMB}}\left(x = \left(1 - \frac{nt_s}{T_s}\right)L\right) \tag{2}
$$

where L is the column length, τ is a time point within a single switch ($\tau = nt_s$) and t_s is the sampling interval. With a switch period, T_s, there is a N sampling instance, (n = 0,1,2, …, N). The superscripts SMB and TMB indicate reading from SMB and TMB respectively. The N time points in SMB have the corresponding position x in TMB, ($x = (1 - (\tau/T_s))L$).

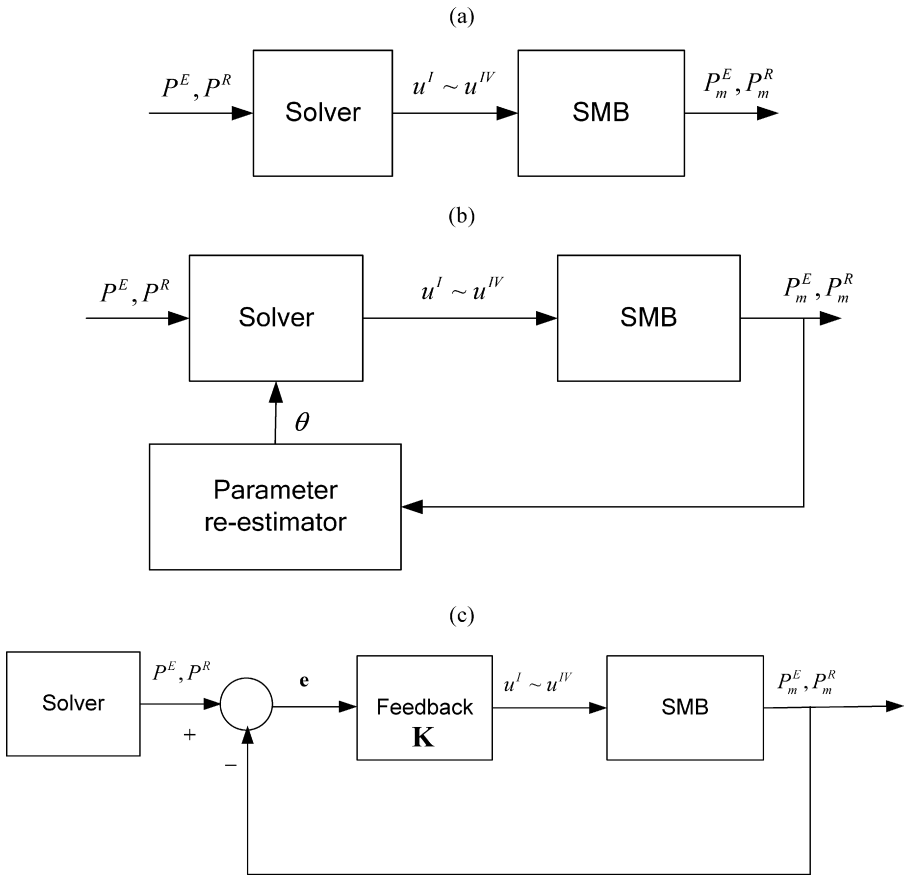

Fig. 2. Design structure: (a) physical based design, (b) updating the physical parameters and then doing the physical based design, and (c) empirical based design.

Using this representation, the reading of concentration from the UV detector of a SMB process can then be mapped onto a TMB profile. Fig. 5 shows how the reconstruction of the wave in zone I and zone IV is done. In Fig. 5a, the dashed line represents the wave profile of TMB in zone I. The solid line is the moving wave of SMB in zone I and the corresponding measured points at the end of zone I are shown in large dots. Thus, at the initial time $\tau = 0$, the point P' of the SMB profile coincides with the point P of the TMB profile; at time $\tau = nt_s$, the point Q' of SMB can be traced back to the position $(1 - (nt_s/T_s))L$ of zone I and it approximates the point Q of TMB; the point R' of SMB at time $\tau = T_s$ approximates the point R of TMB at position $x = 0$. Similarly, in zone IV (Fig. 5b), the point K' of SMB coincides with K of TMB while J' of SMB is related to J of TMB by the same argument, and the point I' of SMB approximates the point I of TMB.

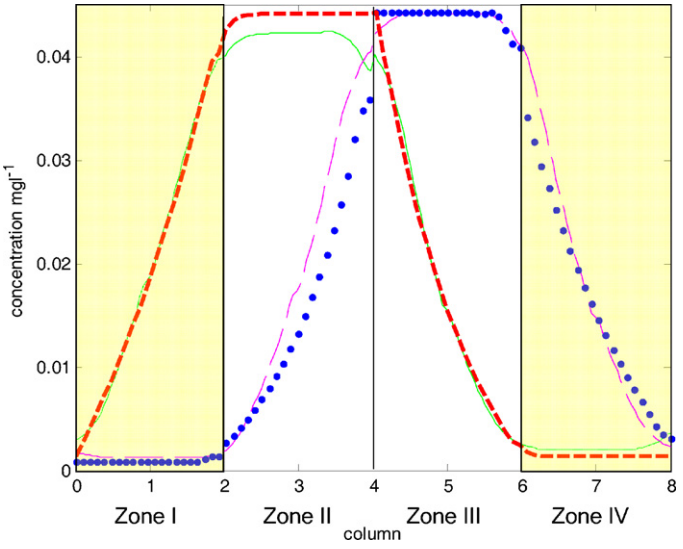

Fig. 3. SMB profiles approximated by TMB.
(.-): more absorbable component for TMB; (..): less absorbable component for TMB solid line: more absorbable component for SMB; (–) less absorbable component for SMB.

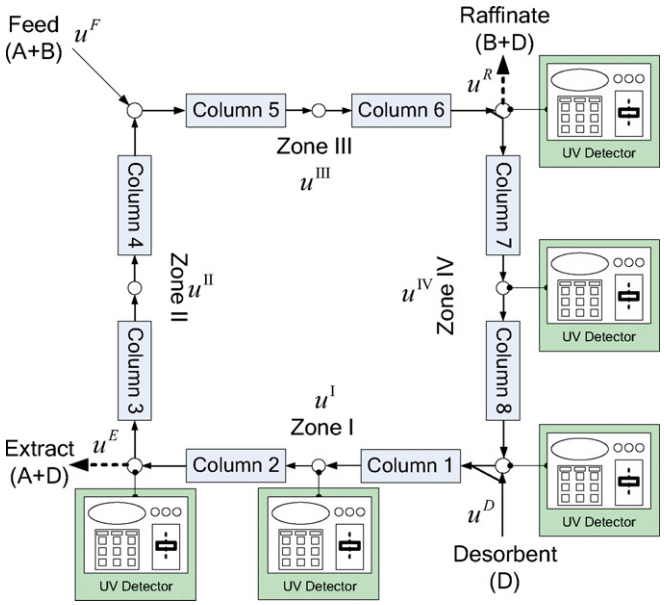

Fig. 4. UV placement.

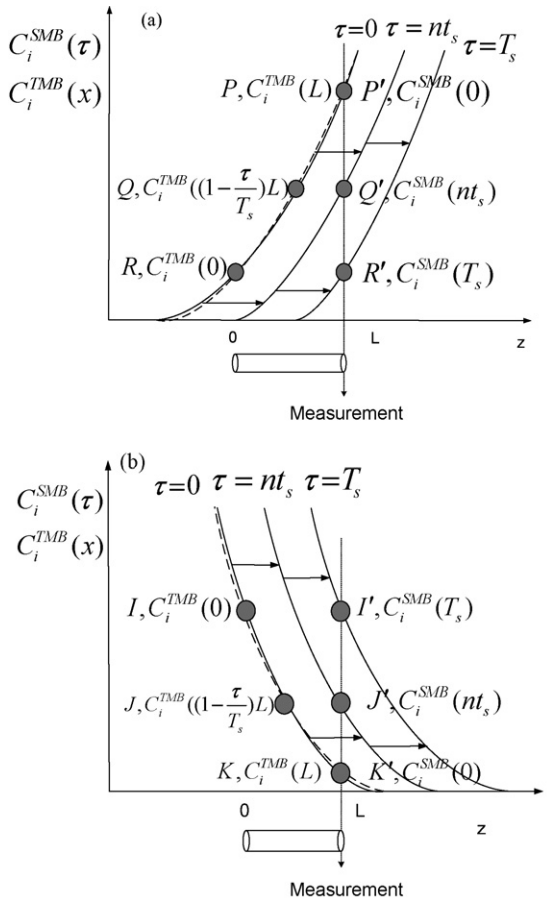

Fig. 5. Wave reconstruction of zone I (a) and zone IV (b).

Fig. 6 shows how a reading from UV signals can be used to construct the wave profile. Fig. 6a, shows the 5 instances in a switch of the SMB profile for both components (thin solid and dashed line respectively). Readings are taken at a fixed position in the SMB unit, each reading represents the SMB profile at different time within a switch and a typical reading of the UV signal is shown for zone I (Fig. 6b) and zone IV (Fig. 6c). For the binary mixture separation, (x) and (o) represent the more adsorbable component and the less adsorbable one respectively. The numbered points represented by the moving SMB profile correspond to the reading from UV. By relating the reading from the time domain of SMB to the spatial domain of TMB using the reasoning relating the SMB and TMB profiles, the profiles in zone I and zone IV can be reconstructed as TMB profiles of the corresponding zone.

3.3. Parameter estimation

In this section, the concentration profile model will be used to solve the physical parameters. First, the fluid and solid phase equations of TMB are defined as,

Fluid phase:

$$\frac{\partial C_i^j}{\partial t} = D_i \frac{\partial^2 C_i^j}{\partial x^2} - (u^j - v)\frac{\partial C_i^j}{\partial x} - \frac{1-\varepsilon_b}{\varepsilon_b} k_{fi}(C_i^j - C_i^{*j}) \tag{3}$$

Solid phase:

$$\varepsilon_p \frac{\partial C_i^{*j}}{\partial t} + (1-\varepsilon_p)\frac{\partial q_i^j}{\partial t} = k_{fi}(C_i^j - C_i^{*j}) + v\varepsilon_p \frac{\partial C_i^{*j}}{\partial x} + (1-\varepsilon_p)v\frac{\partial q_i^j}{\partial x} \tag{4}$$

where C_i^j (mg l^{-1}) is the mobile phase concentration of component i at zone j and C_i^{*j} (mg l^{-1}) is the equilibrium concentration. Note that the superscript representing TMB/SMB is removed because the equation is solved for TMB. q_i^j (mg l^{-1}) is the concentration of component i in zone j at the solid phase in equilibrium. t represents the differentiation with respect to time while x denotes the axial length. D_i (cm^2 min^{-1}) represents axial dispersion coefficient while k_{fi} (min^{-1}) represents the lumped mass transfer coefficient of component i. The lumped mass transfer coefficient is correlated to the pore diffusion coefficient, D_p effective intraparticle diffusion coefficient (cm^2 min^{-1}) and film mass transfer, k_i (cm min^{-1}) as such [3],

$$\frac{1}{k_{f_i}} = \frac{R^2}{15\varepsilon_p D_p} + \frac{R}{3k_i} \tag{5}$$

where R is the particle adsorbent radius. u^j (ml min^{-1}) is the zone flow rate and v (ml min^{-1}) is the solid flow rate in TMB. ε_b is the bed voidage.

Based on the assumption of the separable condition [3], the fluid and the solid phase equations can be combined into

$$\frac{\partial^2 C_i^j}{\partial x^2} - \left(\frac{u^j - (1+P\delta_i)v}{D_i + (Pv^2\delta_i^2/k_{fi})}\right)\frac{\partial C_i^j}{\partial x} = 0 \tag{6}$$

where $\delta_i \equiv \varepsilon_p + (1-\varepsilon_p)K_i$, K_i is the equilibrium constant and $P = (1-\varepsilon_b)/\varepsilon_b$. Since the particles in consideration is non-porous, $\varepsilon_p = 0$; thus $\delta_i = K_i$.

The accompanying boundary equations for zone I and zone IV are as follows:

$$\text{Zone I}: C_i(x=0) = C_{i,\text{in}}^I \text{ and } C_i(x=L) = C_i^{\text{Ext}} \tag{7}$$

$$\text{Zone IV}: C_i(x=0) = C_i^{\text{Raf}} \text{ and } C_i(x=L) = C_{i,\text{out}}^{IV} \tag{8}$$

Solving the differential equation, the solutions for zone I and zone IV concentration profile can be obtained,

$$\text{Zone I}: C_i^I(x) = \frac{C_{i,\text{in}}^I - C_i^{\text{Ext}}}{1-e^{W_i^I L}} e^{W_i^I(x)} + \frac{C_i^{\text{Ext}} - C_{i,\text{in}}^I e^{W_i^I L}}{1-e^{W_i^I L}} \tag{9}$$

$$\text{Zone IV}: C_i^{IV}(x) = \frac{C_i^{\text{Raf}} - C_{i,\text{out}}^{IV}}{1-e^{W_i^{IV} L}} e^{W_i^{IV}(x)} + \frac{C_{i,\text{out}}^{IV} - C_i^{\text{Raf}} e^{W_i^{IV} L}}{1-e^{W_i^{IV} L}} \tag{10}$$

To relate to the measured data from SMB, the spatial representation of TMB as shown in Eqs. (9) and (10) is converted to the time representation of SMB

$$\text{Zone I}: C_i^I(\tau) = \frac{C_{i,\text{in}}^I - C_i^{\text{Ext}}}{1-e^{W_i^I L}} e^{W_i^I((T_s-\tau)/T_s)L} + \frac{C_i^{\text{Ext}} - C_{i,\text{in}}^I e^{W_i^I L}}{1-e^{W_i^I L}} \tag{11}$$

$$\text{Zone IV}: C_i^{IV}(\tau) = \frac{C_i^{\text{Raf}} - C_{i,\text{out}}^{IV}}{1-e^{W_i^{IV} L}} e^{W_i^{IV}((T_s-\tau)/T_s)L} + \frac{C_{i,\text{out}}^{IV} - C_i^{\text{Raf}} e^{W_i^{IV} L}}{1-e^{W_i^{IV} L}} \tag{12}$$

where

$$W_i^j = \frac{u^j - (1+P\delta_i)v}{D_i + (Pv^2\delta_i^2/k_{fi})} \tag{13}$$

contains the parameters to be determined. Using zone I as illustration, W_i^I is first solved for each set of readings. Eq. (13) can be rearranged as

$$(\boldsymbol{x}_i^I)^T \boldsymbol{\theta}_i = y_i^I \tag{14}$$

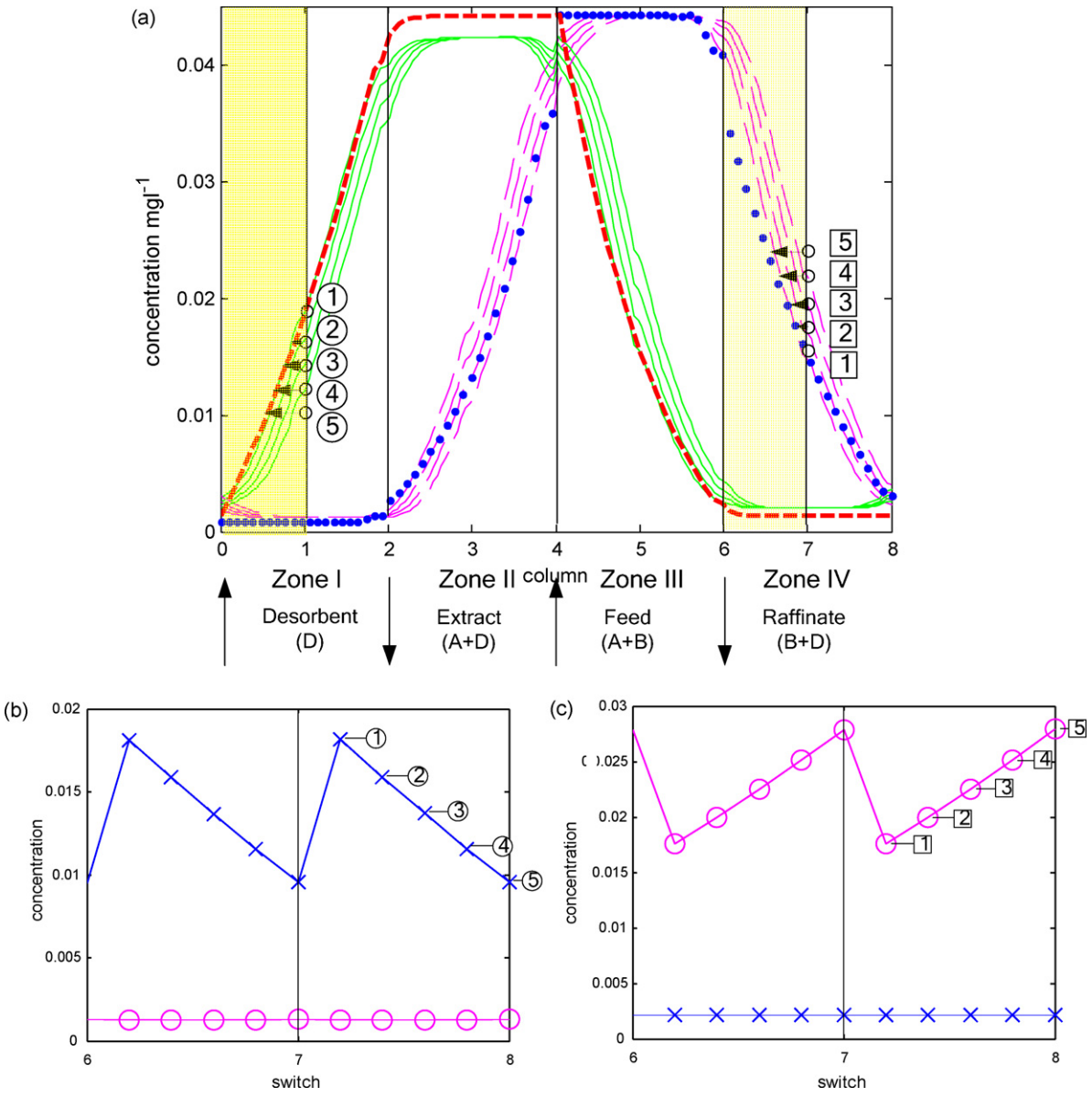

Fig. 6. Wave profile reconstruction: (a) complete profile of SMB and TMB, (.-): more absorbable component for TMB; (..): less absorbable component for TMB; (-): more absorbable component for SMB; (–): less absorbable component for SMB. (b) A typical reading for the operation at the cyclic steady state zone I. (c) A typical reading for the operation at the cyclic steady state zone IV. (x): more adsorbable; (o): less adsorbable.

with

$$\mathbf{x}_i^I = \begin{bmatrix} W_i^I & W_i^I P v^2 & P v \end{bmatrix}^T \tag{15}$$

$$\boldsymbol{\theta}_i = \begin{bmatrix} D_i & \dfrac{\delta_i^2}{k_{fi}} & \delta \end{bmatrix}^T \tag{16}$$

$$y_i^I = \begin{bmatrix} u^I - v \end{bmatrix} \tag{17}$$

With the past operation data, conventional regression can then be carried out to obtain the value of the terms in θ_i and also, with the new output readings, the values are updated recursively.

3.4. Operation design

For the purpose of obtaining the operation condition, the purity is set based on the equation by Xie et al. [11]

$$\beta_A^I = \beta_A^{III} = -\ln\left[\frac{1}{F_C}\left(\frac{1}{P^{\mathrm{Raf}}} - 1\right)\right] \tag{18}$$

$$\beta_B^{II} = \beta_B^{IV} = -\ln\left[F_C\left(\frac{1}{P^{\mathrm{Ext}}} - 1\right)\right] \tag{19}$$

where $F_c(= C_A^F/C_B^F)$ is the concentration ratio of the more adsorbable component to less adsorbable component in the feed. β_i^j is the natural logarithm of the ratio of the highest concentration to the lowest concentration of component i of a standing wave in zone j. It serves as an index of product purity. For the symmetrical profile between zones I, III and zones II, IV, $\beta_A^I = \beta_A^{III}$ and $\beta_B^{II} = \beta_B^{IV}$. The corresponding equation for the four zone flow rates is

$$\begin{aligned} u^j &= (1 + P\delta_A)v + \beta_A^j\left(\frac{D_A}{L^j} + \frac{Pv^2\delta_A^2}{k_{fA}L^j}\right); \quad j = I, III \\ u^j &= (1 + P\delta_B)v + \beta_B^j\left(\frac{D_B}{L^j} + \frac{Pv^2\delta_B^2}{k_{fB}L^j}\right); \quad j = II, IV \end{aligned} \tag{20}$$

where

$$v = \frac{P(\delta_A - \delta_B)}{2((P\beta_A^{III}\delta_A^2/k_{fA}L^{III}) + (P\beta_B^{II}\delta_B^2/k_{fB}L^{II}))} \pm \frac{\sqrt{P^2(\delta_A - \delta_B)^2 - 4((P\beta_A^{III}\delta_A^2/k_{fA}L^{III}) + (P\beta_B^{II}\delta_B^2/k_{fB}L^{II}))((F^{\text{feed}}/\varepsilon_b S) + (\beta_A^{III}D_A/L^{III}) + (\beta_B^{II}D_B/L^{II}))}}{2((P\beta_A^{III}\delta_A^2/k_{fA}L^{III}) + (P\beta_B^{II}\delta_B^2/k_{fB}L^{II}))} \tag{21}$$

After setting the purity and obtaining the β values from Eqs. (18)–(19), v (ml min^{-1}) is calculated using Eq. (21) and then the operation condition which is the zonal velocities, u^j (ml min^{-1}), is obtained from Eq. (20). For each new operation condition, new sets of output readings can be measured. Using this new set of data, the parameters can be recalculated until the parameters converge.

4. Empirical based design method

In the derivation of the solution to the physical model based design, simplified assumptions, like assuming the equivalence of the second order derivative term ($\partial^2 C_i/\partial x^2$) in Eq. (3) to $\partial^2 C_i^*/\partial x^2$ at the steady state, neglecting the effect of the pressure drop and the effect of fluid resistance on the system, can lead to misrepresentation of the system. As a result, if the design is to be done based solely on the physical model, the desired condition will not be achieved. To solve this problem, a subsequent empirical based design is necessary.

4.1. Selection of variables and design of flow rate

The purity is affected by the four zone flow rates as well as the switch time of the process. By Taylor's expansion up to the first order, the relation between the variables at close proximity of a particular point (u^I, u^{II}, u^{III}, u^{IV}, T_s) can be approximated as

$$\begin{aligned} &P^z(u^I + \Delta u^I, u^{II} + \Delta u^{II}, u^{III} + \Delta u^{III}, u^{IV} + \Delta u^{IV}, T_s + \Delta T_s) \\ &\quad = P^z(u^I, u^{II}, u^{III}, u^{IV}, T_s) \\ &\qquad + \left[\frac{\partial P^z}{\partial u^I}\Delta u^I + \frac{\partial P^z}{\partial u^{II}}\Delta u^{II} + \frac{\partial P^z}{\partial u^{III}}\Delta u^{III} + \frac{\partial P^z}{\partial u^{IV}}\Delta u^{IV} + \frac{\partial P^z}{\partial T_s}\Delta T_s\right] \end{aligned} \tag{22}$$

where P^z represents the infinitesimal changes in purity of the extract and raffinate, z = Ext, Raf. To find out which factors affect the purity at the current point, small changes are made to the individual component at a time, and then the sensitivity value ($\partial P^z/\partial u^I$, $\partial P^z/\partial u^{II}$, $\partial P^z/\partial u^{III}$, $\partial P^z/\partial u^{IV}$, $\partial P^z/\partial T_s$) is calculated. Next, the singular value decomposition (SVD) is used to find the factor to be controlled to ensure that the target purity will be attained. It is a method of transforming correlated variables into a set of uncorrelated ones that better expose the various relationships among the original data items. Downs and Moore [12] used SVD to select the best tray temperatures in a distillation process. The matrix of the process change is expressed as the product of three matrices, a **U** matrix, a diagonal **S** matrix and a $\mathbf{V}^T$ matrix, $[\partial P^z/\partial u^I \quad \partial P^z/\partial u^{II} \quad \partial P^z/\partial u^{III} \quad \partial P^z/\partial u^{IV} \quad \partial P^z/\partial T_s\,]^T = \boldsymbol{USV}^T$. The biggest element in the **U** matrix indicates the most sensitive variable. Thus, the strongest variables contributing to the changes of the process can be determined.

The two largest characteristic matrices determine the variables, V_1 and V_2 to be controlled. To select and pair the variables to purity, an analog to the relative gain array (RGA) method in the multivariable process is used. In the multivariable process, RGA is used to determine the optimal input–output variable pairings. It is a normalized form of the gain matrix that describes the impact of each design variable on the output, relative to each design variable's impact on other variables. Therefore, the change in the variables V_1 and V_2 can be represented by

$$\begin{bmatrix} P^{Ext} \\ P^{Raf} \end{bmatrix} = \begin{bmatrix} \dfrac{\partial P^{\text{Ext}}}{\partial V_1} & \dfrac{\partial P^{\text{Ext}}}{\partial V_2} \\ \dfrac{\partial P^{\text{Raf}}}{\partial V_1} & \dfrac{\partial P^{\text{Raf}}}{\partial V_2} \end{bmatrix} \begin{bmatrix} V_1 \\ V_2 \end{bmatrix} \tag{23}$$

Using the normal pairing criteria which select the number closest to 1, a pairing can be obtained

$$\begin{aligned} P_A^{\text{Ext}} &\rightarrow V_1 \\ P_B^{\text{Raf}} &\rightarrow V_2 \end{aligned} \tag{24}$$

where V_1 is related to extract purity, and V_2, to raffinate purity. If fluctuation disturbances exist, the above calculation can be done based on the average values from the greater number of operation to compensate the disturbance.

4.2. Error correction

After pairing, the corrective variables can be determined. The corrective variables is

$$\mathbf{V}(k+1) = \mathbf{V}(k) + \mathbf{K}\mathbf{e}(k) \tag{25}$$

where $\boldsymbol{V}(k+1) = \begin{bmatrix} V_1 \\ V_2 \end{bmatrix}_{k+1}$ represents the subsequent variables as with $\boldsymbol{V}(k) = \begin{bmatrix} V_1 \\ V_2 \end{bmatrix}_k$ representing the variables and the weighting as $\boldsymbol{K} = \begin{bmatrix} k_1 & 0 \\ 0 & k_2 \end{bmatrix}$.

The error is

$$\mathbf{e}(k) = \begin{bmatrix} e_B(k) \\ e_A(k) \end{bmatrix} \tag{26}$$

where $e_A(k)$ and $e_B(k)$ represent the errors between desired purity and actual purity

$$e_A(k) = P_A^{\text{Ext}}(k) - P_{m,A}^{\text{Ext}}(k) \tag{27}$$

$$e_B(k) = P_B^{\text{Raf}}(k) - P_{m,B}^{\text{Raf}}(k) \tag{28}$$

The correction is then carried out until desired purity is achieved.

With reference to Fig. 2, the proposed method can be summarized as follows.

4.2.1. Phase I: physical based design

Step 1: Designate a preliminary flow from the prior knowledge of parameters (Eqs. (18)–(21)).
Step 2: Conduct the SMB operation under the design condition and collect the measured concentrations from the extract and raffinate ports with UV detectors.
Step 3: Calculate new sets of parameters by regression with new output data (Eqs. (14)–(17)).
Step 4: Calculate the new operation condition with the newly obtained parameters and conduct the SMB operation (Eqs. (18)–(21)).
Step 5: If purity reach the desired value, stop; otherwise, go back to step 3 and carry out iterative calculation of the parameters

with the new sets of data. Step 3 to 5 are repeated until the parameter value converges and then go to step 6.

4.2.2. Phase II: empirical based design

Step 6: Select the pairing of the variables. (Eq. (24)).
Step 7: The new operation condition is calculated iteratively using the error between the predicted output and the actual output (Eq. (25)) and is continued until the design specification is reached.

5. Results and discussion

The proposed method is simulated on a virtual eight-column SMB process. The purpose is to demonstrate the need for calculation and design of the process by an iterative approach. For a system with a priori knowledge of the system, the aim is to demonstrate the need to recalculate the parameter and the advantage of a combined approach of physical and empirical design. A simulation whose corrective action is only based on the empirical approach without parameter recalculation is shown. This is followed by a simulation in which a combined approach of recalculation of the process parameters is shown. The two methods are contrasted to show the advantages of the latter.

5.1. Simulation work

For the simulation system, a linear isotherm system of the SMB process is used. The true system parameters are $C_A^F = C_B^F = 0.05\%$ (w/v), $D_A = 3.852\,\text{cm}^2\,\text{min}^{-1}$, $D_B = 3.808\,\text{cm}^2\,\text{min}^{-1}$ $k_{fA} = 4.6644\,\text{min}^{-1}$, $k_{fB} = 2.6676\,\text{min}^{-1}$, $H_A = 0.38$, $H_B = 0.12$. Note that H_i is the Henry's coefficient for each component. The objective is to achieve 98% of purity. For the purpose of demonstration, it is assumed that prior knowledge of the system parameters includes $D_A = 4.23\,\text{cm}^2\,\text{min}^{-1}$, $D_B = 4.62\,\text{cm}^2\,\text{min}^{-1}$, $k_{fA} = 5.17\,\text{min}^{-1}$, $k_{fB} = 3.05\,\text{min}^{-1}$, $H_A = 0.5$, and $H_B = 0.02$. They differ from the true system parameters and thus will result in a discrepancy from the designated purities.

5.2. Design based on the empirical approach only

Using the initial sets of parameters, the operation condition can be calculated using Eqs. (18)–(21) and the system is operated in a simulation. The extract and raffinate purity obtained are 88% and 84% respectively, which does not meet the specification of 98% purity. For the purpose of illustration, the triangle theory has been used to draw the region of complete separation for the linear isotherm system [2]. The parameter m_j is the ratio of fluid phase mass flow rate to the adsorbed phase mass flow rate. In the triangular plot (Fig. 7), the dash line region represents the region with the initial inaccurate parameters whereas the solid line region is the region with accurate parameters. In Fig. 7, the initial operation point represented by Δ does not fall into the solid line triangle, which represents the high separation region.

Corrective flow rates are to be calculated solely based on empirical approach. Based on the method outlined in Section 4, the SVD value calculated is

$$\mathbf{U} = \begin{bmatrix} 0.7340 & -0.6281 \\ 0.6050 & 0.7750 \\ -0.0043 & -0.0014 \\ -0.0187 & -0.0633 \\ 0.3081 & -0.0291 \end{bmatrix}, \mathbf{S} = \begin{bmatrix} 0.6072 & 0 \\ 0 & 0.5259 \end{bmatrix},$$

$$\mathbf{V}^T = \begin{bmatrix} 0.6121 & 0.7908 \\ -0.7908 & 0.6121 \end{bmatrix}$$

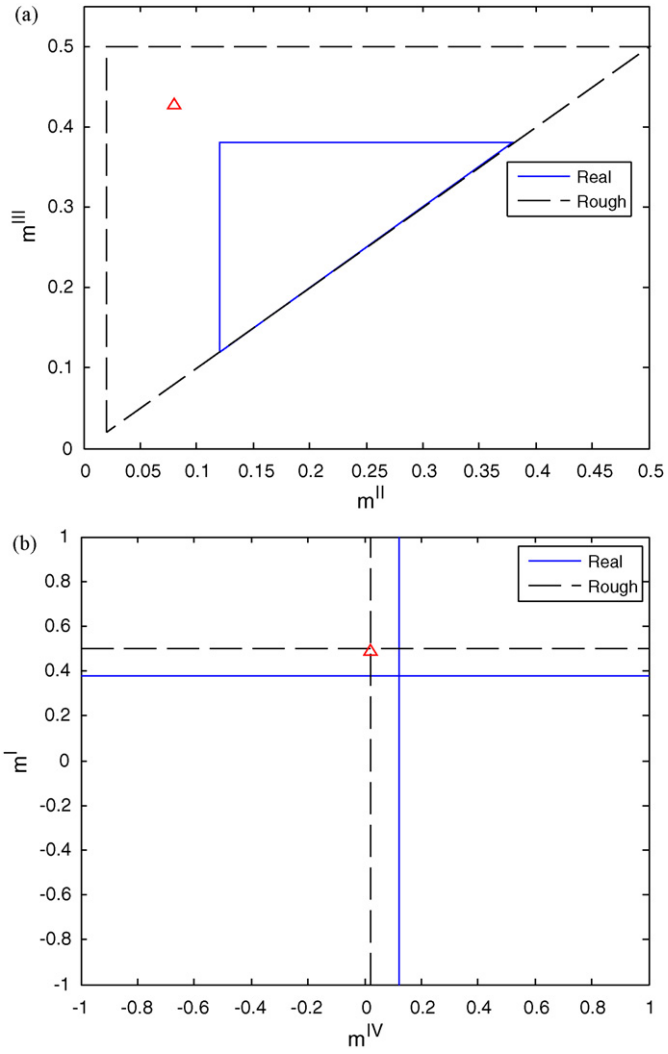

Fig. 7. (a) m^{II} and m^{III} plot and (b) m^{I} and m^{IV} plot for an initial set of data, where dash line region is obtained with inaccurate parameters and the solid line region is obtained with accurate parameters.

The **U** matrix shows that the largest characteristic flow affecting the purity is zone I and zone II flow rates. Based on the characteristic gain values calculation, the following value is obtained,

$$\begin{bmatrix} \frac{\partial \hat{P}_A^{\text{Ext}}}{\partial u^I} & \frac{\partial \hat{P}_A^{\text{Ext}}}{\partial u^{II}} \\ \frac{\partial \hat{P}_B^{\text{Raf}}}{\partial u^I} & \frac{\partial \hat{P}_B^{\text{Raf}}}{\partial u^{II}} \end{bmatrix} = \begin{bmatrix} -0.0016 & 1.0016 \\ 1.0016 & -0.0016 \end{bmatrix}$$

Selecting the value closest to 1 results in pairing of extract purity to the flow rate in zone II and raffinate purity to the flow rate in zone I. The sequential experimental results are obtained as shown in Fig. 8.

In Fig. 8, for the change in purity with time, it can be seen that the target purity still cannot be achieved. The triangular plot confirms this result. In Fig. 9, the path of the correction, with the triangle (Δ) representing the initial point does not drive the process into the actual region for high purity separation. Due to lack of correction to the process parameters, the operation is not driven to the correct high separation region and the corrective action is not able to overcome this.

Table 1
Regression of parameters for 6 iterations.

Count	$[H_A\ H_B]$	$[K_{fA}\ K_{fB}]$	$[D_A\ D_B]$	$[u^I\ u^{II}\ u^{III}\ u^{IV}\ T_s]$	$[P^E\ P^R]$
0	[0.5 0.02]	[5.17 3.05]	[4.23 4.62]	[3.3 2.39 3.16 2.26 16.5]	[0.88 0.84]
1	[0.382 0.107]	[0.373 0.035]	[0.374 1.007]	[3.27 2.53 3.15 2.40 16]	[0.93 0.91]
2	[0.377 0.104]	[0.349 0.027]	[0.435 0.270]	[3.40 2.67 3.25 2.48 15.4]	[0.95 0.93]
3	[0.372 0.120]	[0.359 0.962]	[0.813 4.156]	[4.05 3.12 3.84 3.01 13]	[0.93 0.95]
4	[0.383 0.120]	[18.71 0.253]	[3.431 3.817]	[3.43 2.69 3.27 2.55 15.1]	[0.93 0.95]
5	[0.382 0.120]	[13.06 0.248]	[3.466 3.816]	[3.47 2.73 3.32 2.58 15]	[0.95 0.94]
6	[0.382 0.121]	[14.85 0.245]	[3.506 3.815]	[3.41 2.87 3.25 2.71 14.9]	[0.96 0.95]

5.3. Design based on the hybrid approach

The proposed hybrid approach is used in the same condition mentioned previously. From the empirical approach, the shortcoming of not updating the process parameters is seen, to this end, this second approach re-evaluate the process parameters with the new operation measurements. With different sets of operation data from close proximity of the initial design condition, regression is carried out from Eqs. (14)–(17) to obtain the actual parameters. Then the new operating condition is directly updated with Eqs. (18)–(21). The sequential updated parameters and the corresponding design results are shown in Table 1 with count 0 representing the initial point. Note that in the event that parameters are unknown, the above procedures are applicable for estimation. On the other hand, even with prior knowledge, the historical data may not represent the current status due to the changes in the process. The iterative procedure is needed to update the parameters.

After 6 counts of regression, the parameters converge. Although design purity is not attained, the first point of the operation after the parameters converge is within the high purity region in the triangular plot (shown in Fig. 10). In Fig. 10, the triangle (Δ) represents the initial point for the prior sets of parameters (which are inaccurate) and (O) represents the first point after parameter calculation. Here the purity specification is still not attained and the contributing factor is that the second order derivative of mobile phase concentration is assumed to be equal to the mobile phase equilibrium concentration when the stationary phase and the mobile phase are at equilibrium. Fig. 11 shows the difference with and without the assumption. Nevertheless, it can be observed that the first point after parameter calculation (O) does fall within the high purity region.

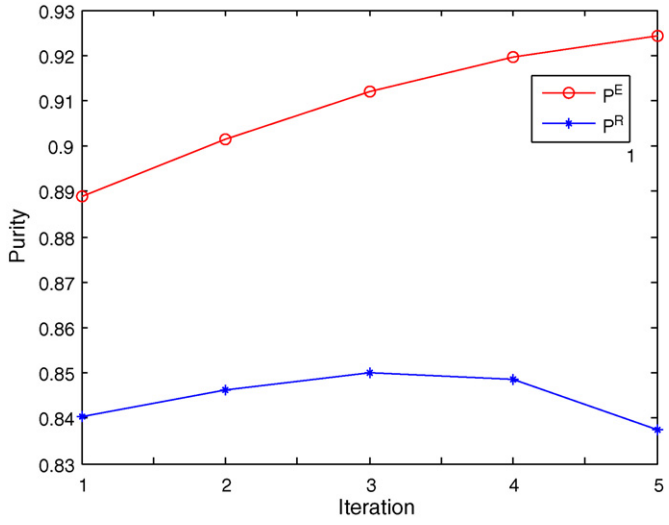

Fig. 8. Purity change with time based on the empirical model instead of parameter estimation.

To remedy the model mismatch and enhance the product qualities, the empirical based approach is then applied. The SVD calculation for this case is

$$\mathbf{U} = \begin{bmatrix} 0.9628 & 0.0953 \\ 0.0514 & 0.6263 \\ -0.1127 & 0.2473 \\ 0.1175 & -0.7316 \\ 0.2093 & -0.0480 \end{bmatrix}, \mathbf{S} = \begin{bmatrix} 0.0612 & 0 \\ 0 & 0.0320 \end{bmatrix},$$

$$\mathbf{V}^T = \begin{bmatrix} 0.0127 & -0.9999 \\ -0.9999 & -0.0127 \end{bmatrix}$$

For this second case, the **U** matrix shows that the largest characteristic flow affecting the purity is zone I and zone IV flow rates. Similarly, the characteristic gain values calculation is carried out

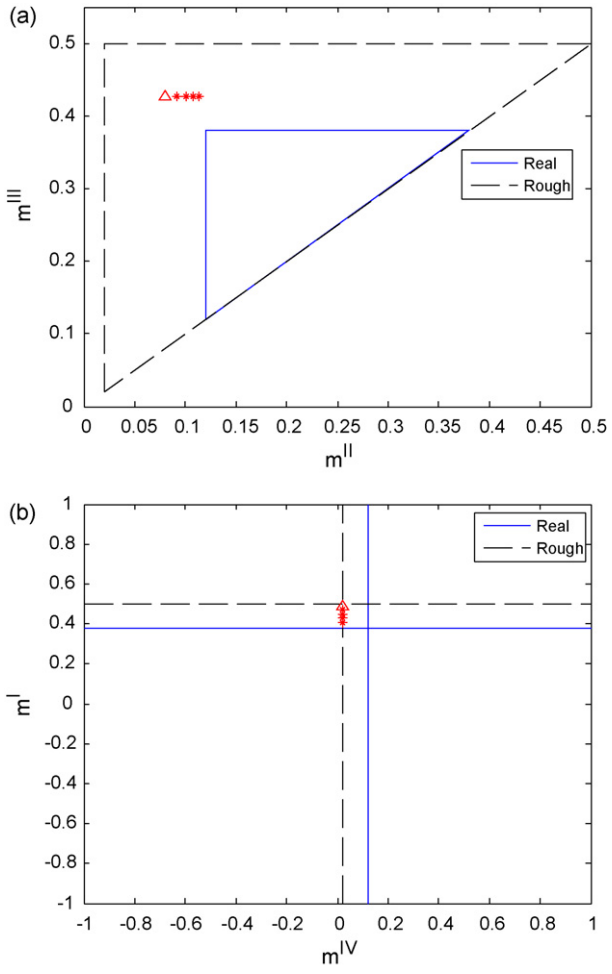

Fig. 9. (a) m^{II} and m^{III} plot and (b) m^I and m^{IV} plot showing the path of the correction. (Δ: initial point, *: subsequent operation point).

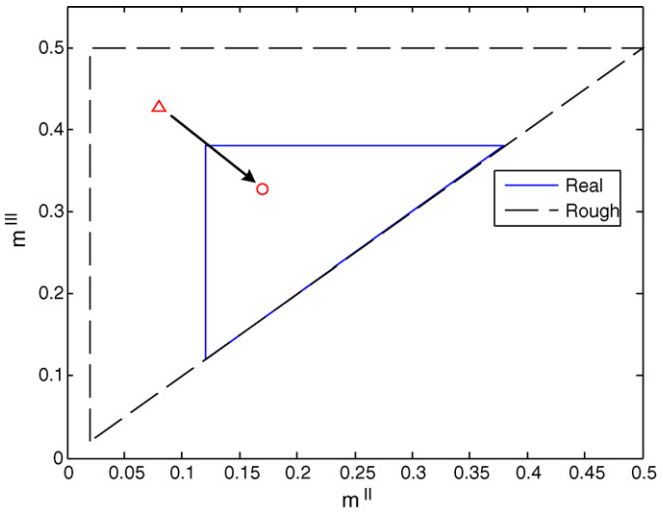

Fig. 10. The start point is close to the high purity region (Δ: initial point without parameter calculation, ○: the first point after parameter calculation).

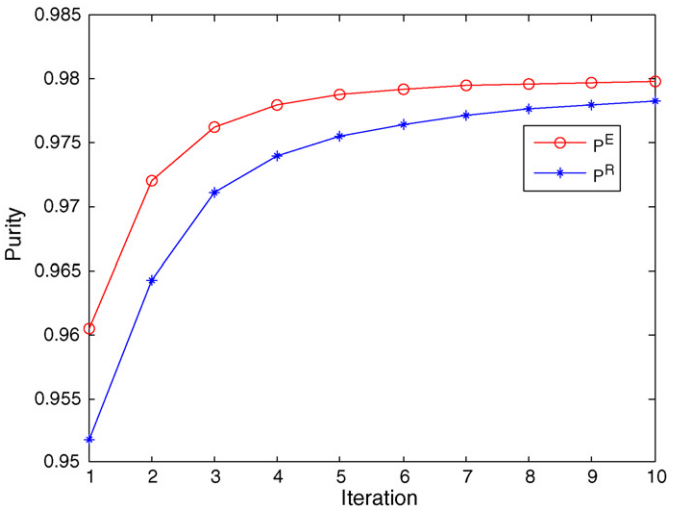

Fig. 12. Purity profile after parameter estimation. (ɵ: extract purity, *: raffinate purity).

with the following value obtained,

$$\begin{bmatrix} \frac{\partial \hat{P}_A^{\mathrm{Ext}}}{\partial u^I} & \frac{\partial \hat{P}_A^{\mathrm{Ext}}}{\partial u^{II}} \\ \frac{\partial \hat{P}_B^{\mathrm{Raf}}}{\partial u^I} & \frac{\partial \hat{P}_B^{\mathrm{Raf}}}{\partial u^{II}} \end{bmatrix} = \begin{bmatrix} 0.0113 & 0.9887 \\ 0.9887 & 0.0113 \end{bmatrix}$$

which point to a pairing of extract purity to the flow rate in zone IV and the raffinate purity to the flow rate in zone I. The next phase of correction is carried out and the process is able to achieve the design specification.

Fig. 12 shows that purity of extract reaches 98% and raffinate, 97.8%. They are very close to the design specifications. Compared to the previous experiment where no parameter estimation is carried out, a vast improvement is shown. To summarize the results, given initial parameters which may not be a true reflection of the real process, it is necessary to recalculate the parameters. The corrected parameters allow operation within or close to the good separation region. However, the inherent model error may still hinder the achievement of the desired target. The use of the corrective action based on the feedback data of the measured output gives rise to a corrective action that eliminates the discrepancy and enables the process to operate at designated product purity.

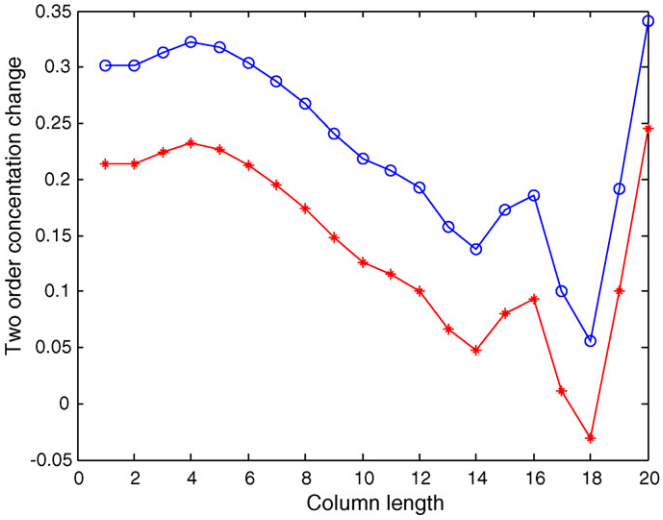

Fig. 11. The second derivative difference. (*): $\partial^2 C_i/\partial x^2$ the second order derivative of mobile phase concentration. (o): $\partial^2 C_i^*/\partial x^2$ the mobile phase equilibrium concentration when the stationary phase and the mobile phase are at equilibrium.

6. Conclusion

A novel scheme for design of the SMB process has been proposed. The design of the flow rates depending on the knowledge of the parameters for the process is crucial for high purity separation. The proposed method combines a two-phase method in the design. It offers the following benefits:

1. *On-line parameter estimation*: Changes in the operation of the process mean the parameters determined offline may no longer be a true reflection of the process and need to be re-determined. Carrying out an on-line design is the most effective way to ensure that the designated purity is not affected by process changes.
2. *The hybrid design method eliminates model uncertainty*: The proposed method combines a physical based method and an empirical based method. The physical based method allows calculation of the operation condition close to the actual point. Model discrepancy which results in the unattainable target is rectified by a correction action based on the errors between the target and actual purities.

The proposed method has been conducted in a virtual eight-column SMB process. The results reaffirm that parameter calculation and the corrective action are necessary to attain the designated specifications. The continuing research plan will include the implementation of the proposed method on the actual SMB experimental unit to assess its applicability in the real process. In the current work, the dynamics of the system is not considered. Nevertheless, in the next stage, it is a good idea to take into account the dynamics of the system while the desired steady state target is designed.

Acknowledgments

This work is supported by the Center-of-Excellence (COE) Program on Membrane Technology from the Ministry of Education (MOE), ROC, and to the project Toward Sustainable Green Technology in the Chung Yuan Christian University, Taiwan, under grant CYCU-98-CR-CE and the National Science Council (NSC). These are gratefully acknowledged.

References

[1] S. Mun, N.-H.L. Wang, Y.-M. Koo, S.C. Yi, Pinched wave design of a four-zone simulated moving bed for linear adsorption systems with significant mass-transfer effects, Ind. Eng. Chem. Res. 45 (2006) 7241–7250.

[2] G. Storti, M. Mazzotti, M. Morbidelli, S. Carra, Robust design of binary countercurrent adsorption separation processes, AIChE J. 39 (1993) 471–492.

[3] Z. Ma, N.-H. Wang, Standing wave analysis of SMB chromatography: linear system, AIChE J. 43 (1997) 2488–2508.

[4] A. Toumi, S. Engell, M. Diehl, H.G. Bockb, J. Schlöder, Efficient optimization of simulated moving bed processes, Chem. Eng. Process. 46 (2007) 1067–1084.

[5] Y. Kawajiri, L.T. Biegler, Large scale nonlinear optimization for asymmetric operation and design of Simulated Moving Beds, J. Chromatogr. A 1133 (2006) 226–240.

[6] Z.Z. Zhang, M. Mazzotti, M. Morbidelli, Multiobjective optimization of simulated moving bed and Varicol processes using a genetic algorithm, J. Chromatogr. A 989 (2003) 95–108.

[7] P.V. Lima, P.M. Saraiva, A semi-mechanistic model building framework based on selective and localized model extensions, Comput. Chem. Eng. 31 (2007) 361–373.

[8] M. Heertjes, T. Tso, Nonlinear iterative learning control with applications to lithographic machinery, Control Eng. Pract. 15 (2007) 1545–1555.

[9] J. Chen, K.-C. Lin, C.-K. Kong, Application of the batch-to-batch and within-batch iterative optimal design strategy for pervaporation processes, Sep. Pur. Technol. 55 (2007) 265–273.

[10] T. Kleinert, J. Lunze, Decentralised control of chromatographic simulated moving bed processes based on wave front reconstruction, J. Process Control 18 (2008) 780–796.

[11] Y. Xie, D. Wu, Z. Ma, N.-H.L. Wang, Extended standing wave design method for simulated moving bed chromatography: linear systems, Ind. Eng. Chem. Res. 39 (2000) 1993–2005.

[12] J.J. Downs, C.F. Moore, Steady state gain analysis for azeotropic distillation, in: Proc. JACC, Charlottesville, VA, 1981.